Environmental Science Nano

Field-deployable Measurement of Soil Extracellular Enzyme Activity Using Surface-enhanced Raman Spectroscopy

Journal:	*Environmental Science: Nano*
Manuscript ID	EN-COM-04-2025-000382.R1
Article Type:	Communication

ENVIRONMENTAL SIGNIFICANCE STATEMENT

This study pioneers a novel application of surface-enhanced Raman spectroscopy (SERS) for rapid, field-deployable quantification of soil extracellular enzyme activity—a key indicator of soil health and organic matter transformation. By integrating rapid SERS detection with partial least square (PLS) modeling, we developed a portable, low-cost approach for monitoring enzymatic activity in highly heterogeneous soil samples within 30 minutes, rather than the 24 hours required by conventional colorimetric assays. Bridging enzyme concentration with microbial activity, this method overcomes the spatial and temporal limitations of traditional laboratory assays and enables scalable, field-based assessment of soil health. This work establishes a foundation for data-driven monitoring of soil biogeochemical processes and promotes broader adoption of advanced sensing tools in complex environmental conditions.

Field-deployable Measurement of Soil Extracellular Enzyme Activity Using Surface-enhanced Raman Spectroscopy

Hanwei Wang,[1,2] Lahiru Gamage,[3] Jianwei Li,*[3] Haoran Wei*[1,2]

1. *Environmental Chemistry and Technology, University of Wisconsin−Madison, 660 N. Park St., Madison, Wisconsin 53706, USA*
2. *Department of Civil and Environmental Engineering, University of Wisconsin−Madison, Madison, Wisconsin 53706, USA*
3. *Department of Environmental Sciences, Tennessee State University, Nashville, TN 37209, USA*

*Corresponding author. E-mail: jli2@Tnstate.edu, haoran.wei3@wisc.edu; Tel: +1 (615) 963-1523, +1 (608) 263-6278

In preparation for ***Environmental Science: Nano***

ABSTRACT

Soil is essential for maintaining ecological function, productivity, and environmental balance, thereby supporting human society. As an important indicator of soil health, extracellular enzyme activities provide valuable insights into the biological transformation of soil organic matter. However, conventional colorimetric methods are time-consuming, labor-intensive, and impractical for large-scale or field-based monitoring. In this study, we demonstrate for the first time the use of surface-enhanced Raman spectroscopy (SERS) to monitor the oxidation kinetics of L-3,4-dihydroxyphenylalanine (L-DOPA), catalyzed by two representative enzymes: horseradish peroxidase (HRP) and polyphenol oxidase (PPO). By coupling SERS detection with partial least squares (PLS) modeling, we established quantitative correlations between Raman spectral data and enzyme concentration (R^2 = 0.983 for HRP; R^2 = 0.865 for PPO). This model was further applied to 117 soil samples collected from diverse ecosystems in Nashville, TN, to correlate SERS spectra with enzyme activity measured by standard laboratory assays. Despite the inherent heterogeneity of real soil samples, SERS-based predictions of enzyme activity showed strong agreement with conventional measurements (R^2 = 0.753). All SERS measurements were performed using a handheld Raman spectrometer, underscoring the potential for rapid, *in-situ* deployment. This study introduces a scalable, cost-effective paradigm for real-time monitoring of soil enzyme activity, providing a foundation for advanced environmental sensing and enabling data-driven assessments of soil biogeochemical processes in the field.

KEYWORDS

Horseradish peroxidase, polyphenol oxidase, partial least square regression, soil organic matter, free radicals, SERS

INTRODUCTION

Soil plays a pivotal role in sustaining life and maintaining ecological balance. Its health is vital to addressing contemporary challenges such as food security, biodiversity loss, and climate change.[1] Soil organic matter (SOM) serves as a cornerstone of soil health and is a crucial component of the soil ecosystem. It is made up of a diverse array of organic materials derived from living organisms, including plants and microbial debris, microbial biomass, etc.[2] The degradation of these carbon-rich macromolecules (e.g., cellulose and lignin) is driven by extracellular enzymes secreted by microbes and released into the soil.[3, 4] Therefore, extracellular enzyme activities provide valuable insights into the transformation of SOM.

Currently, colorimetric *in vitro* assays are commonly used for measuring enzyme activities in soil.[5, 6] However, this method cannot be performed *in situ* and in real time, as it requires lengthy incubation under delicate laboratory conditions. Additionally, this laboratory-based method is time-consuming and labor-intensive, making it unsuitable for large-scale data collection required to develop models that disentangle the mechanisms underlying the complex soil microbial processes.[7] Therefore, there is a strong demand for sensors that are more cost- and time-efficient for monitoring the temporal and spatial variability of soil enzyme activities across fields. Surface-enhanced Raman spectroscopy (SERS) has demonstrated single-molecule sensitivity by substantially enhancing the Raman cross sections of target analytes near the surfaces of plasmonic nanoparticles.[8-10] In addition, SERS provides bonding vibrational fingerprints of chemicals within seconds, making it an ideal tool for reporting real-time variations in SOM under the influence of soil enzymes.

In this study, we applied SERS for the first time to monitor the oxidation kinetics of SOM catalyzed by two typical soil extracellular enzymes, horseradish peroxidase (HRP) and polyphenol oxidase

(PPO). L-3,4-dihydroxyphenylalanie (L-DOPA) was used as a model SOM probe, which is commonly employed in benchmark colorimetric enzyme activity assays. A partial least squares (PLS) model was developed to establish the relationship between extracellular enzyme concentration and SERS spectrum of the SOM probe. Our results demonstrated excellent performance of the PLS model to predict pure enzyme concentration based on the SERS spectrum of L-DOPA. The model's performance remained satisfactory when applied to real soil samples from various locations, including grasslands, farmlands, woodlands, wetlands, and gardens. This study provides mechanistic insights into enzyme-driven oxidation kinetics of SOM and introduces a new approach for rapid and cost-effective measurement of soil enzyme activities.

MATERIALS AND METHODS

Chemicals. Gold(III) chloride trihydrate (≥99.9%), 3,4-dihydroxy-L-phenylalanine (L-DOPA, ≥98%), acetic acid (≥99%), and iron(II) sulfate heptahydrate (≥99%) were purchased from Sigma-Aldrich (St. Louis, MO, USA). Hydrogen peroxide (27-30% w/w), sodium acetate anhydrous (≥99.0%), sodium citrate dihydrate (≥99.0%), and potassium sulfate (≥99.0%) were purchased from Fisher Scientific (Waltham, MA, USA). Horseradish peroxidase (HRP) and polyphenol oxidase (PPO) were obtained from Abnova (Taipei, Taiwan) and stored at -20 °C. Enzyme solutions were prepared by dissolving HRP or PPO in acetate buffer (50 mM, pH 5.0). Fresh enzyme and L-DOPA solutions were made daily for use. All solutions were prepared using ultrapure water (18.2 MΩ•cm) generated by a Milli-Q Advantage Water Purification System (Millipore, Billerica, MA, USA).

Soil samples. A total of 108 soil samples (depth: 0-10 and 10-20 cm) were collected from sixteen sites at the Tennessee State University campus farm area representing different land uses and

ecosystem types, such as switchgrass and gamagrass croplands, animal farm, wetland, residential lawn, urban soil close to main road, urban forests, community garden, and bare ground. Sample information was summarized in Table 1. All soil samples were assayed for soil extracellular enzyme activities following the same procedure as detailed in the following sections, which will be used as the ground truth data against the measurements derived from the Raman spectroscopic measurements.

Table 1. Site characteristics and soil collections in the TSU campus area in Nashville TN

Ecosystem type	Sampling location	Soil depth	# of samples
Bioenergy cropland	Switchgrass warming experiment field at TSU	0-10 cm, 10-20 cm	18
	Switchgrass and gamagrass fertilization experiment field at TSU	0-10 cm, 10-20 cm	12
Agriculture	Croplands in suburban areas	0-10 cm, 10-20 cm	19
	Animal farm at TSU	0-10 cm, 10-20 cm	18
Forest	Soils under trees with less intensive disturbance	0-10 cm, 10-20 cm	6
	Forested patch in suburban area	0-10 cm, 10-20 cm	6
Wetland	Wetland next to the farm building	0-10 cm, 10-20 cm	6
Urban area	TSU community garden	0-10 cm	6
	A residential house in Downtown Nashville	0-10 cm	6
	Roadside grassland	0-10 cm, 10-20 cm	6
	Soils in crevices	0-10 cm, 10-20 cm	6
Bare ground	Bare ground	0-10 cm	6

Gold nanoparticle (AuNP) synthesis. AuNPs were synthesized using the seed-mediated growth method detailed in our previous study and Text S1.[11] The as-synthesized AuNPs are uniform

spheres with a diameter of 43±5 nm based on transmission electron microscopy (TEM) imaging analysis.[12] UV–vis spectroscopy further confirmed their optical properties, showing a characteristic surface plasmon resonance peak at 531 nm.[12]

***In-situ* sensing of L-DOPA oxidation kinetics catalyzed by enzymes.** An aliquot of 0.2-mL L-DOPA solution (25 mM) and 0.8-mL enzyme solution (either HRP or PPO) was added successively to 3 mL of AuNP suspension. For PPO experiments, this point was designated as "0 min", whereas for HRP experiments, "0 min" was marked after the addition of 0.04 mL of H_2O_2 solution (0.3% w/w). The enzyme-catalyzed oxidation kinetics of L-DOPA were monitored at 15-min intervals for up to 1 hr using a handheld Raman spectrometer. Enzyme concentrations of 0, 1, 5, 15, 30, 60, and 100 mg/L were used, and all experiments were performed in triplicate to ensure reproducibility.

Control experiments were conducted to evaluate the role of each individual component (i.e., HRP, L-DOPA, and H_2O_2) or a combination of two components in the oxidation kinetics of L-DOPA. In single negative controls, one of the three components was replaced with a blank solution, while the other two remained unchanged. For double negative controls, two of the three components were replaced with blank solutions, leaving the remaining one unchanged. The blank solutions consisted of acetate buffer (50 mM, pH 5.0) for HRP and Milli-Q water for L-DOPA and H_2O_2. Consistent with the enzyme activity analysis protocol, the three components were mixed first before being added to AuNP suspension. Furthermore, a Fenton reaction was designed as a positive control for comparison with HRP-catalyzed L-DOPA oxidation. Aliquots of 3-mL AuNP suspension, 0.2-mL L-DOPA solution (25 mM), 0.8-mL $FeSO_4$ solution (0.1 mM), and 0.04-mL H_2O_2 solution (0.3% w/w) were mixed in a sample vial, and Raman spectra were recorded every 15 min for 1 hr.

Enzyme activity analysis of soil samples. Soil samples were collected from farmlands, grasslands, woodlands, wetland, and gardens in Nashville, TN and immediately transported to the laboratory at Tennessee State University. All the samples were sieved via 2-mm sieve after rocks, roots, and other visible debris were removed (Fig. 1); and analyzed on the same day of collection to ensure freshness. Soil oxidase activities were quantified following published protocols.[13, 14] Sample suspensions were prepared by placing 1.0 g of soil in a 125-mL Nalgene bottle. Acetate buffer (50 mM, pH 5) was added to the bottle and the resulting suspension was homogenized using a Brinkmann Polytron for approximately 1 min (Fig. 1). Additional buffer was added to the bottle to bring the final suspension volume to 125 mL.

The assays of enzyme activity were conducted in clear 96-well microtiter plates. The assay design included 8 wells of blank control (250 µL buffer), 8 wells of substrate control (200 µL buffer + 50 µL L-DOPA), 8 wells of sample control (200 µL soil slurry + 50 µL buffer) and 16 wells of assay (200 µL soil slurry + 50 µL L-DOPA) for each soil sample. HRP assays received an additional 10 µL of H_2O_2 (0.3% w/w) in all wells. The plates were placed in an Echotherm incubator at 20 ºC for 18 h. Activity was then quantified by measuring absorbance at 450 nm. The average of enzyme activities from eight replicated wells in one assay plate was derived to represent the enzyme activity. Laboratory tests were conducted, and specific protocols were optimized to secure sufficient soil mixing by sealing soil samples in a plastic Ziploc bag, repeatedly pressing, shaking, and mixing with hands. As a result, the variation of each measurement (i.e., coefficient of variation) in multiple tests ranged from 2~8%. All enzyme activities were calculated as µmol activity h^{-1} g $soil^{-1}$. Raman sensing experiments were conducted in paralell with enzyme activity assays. Similarly, an aliquot of 0.2-mL L-DOPA solution, 0.8-mL soil slurry, and 0.04-mL H_2O_2 solution were mixed, followed by the addition of 3-mL AuNP suspension. After 1 hr, 0.2 mL of K_2SO_4

solution (300 mM) was added to each sample to induce SERS hot spot formation prior to Raman spectral acquisition (Fig. 1). This K_2SO_4 concentration was selected based on our previous study,[12] as it effectively promotes hot spot formation without causing rapid colloidal destabilization.

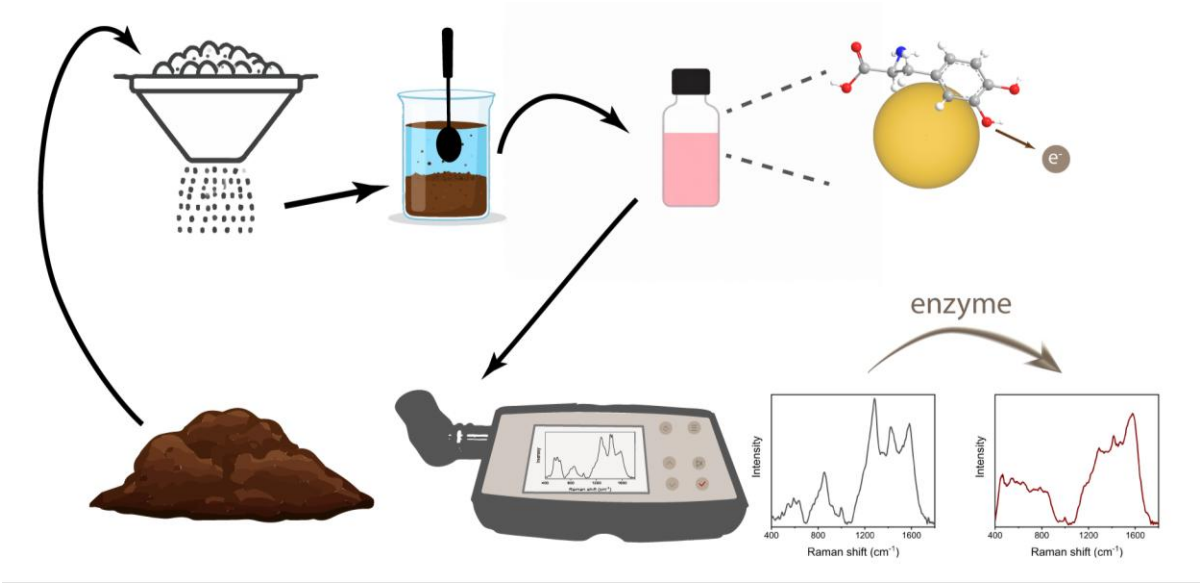

Figure 1. Schematic of soil sample treatment and SERS measurements.

Instrumentation. All Raman spectra were acquired between 400 and 1800 cm^{-1} using a handheld Raman spectrometer (Cora 100, Anton Paar GmbH, Graz, Austria). The excitation source is a 785 nm laser with a maximum power intensity of 300 mW. Raman scatterings were detected by a linear charge-coupled device array. The absorbance was measured using a FilterMaxF5 Multi-Mode Microplate Reader (Molecular Devices, CA, USA) for enzyme activity assay.

Partial least square (PLS) modeling. Before PLS modeling, all the Raman spectral data were baseline-corrected and normalized to the band with the highest intensity. PLS regression was then performed with a variable number of principal components (n = 1, 2, 3…), correlating enzyme concentration with the respective Raman spectrum. The final model was established using the optimal component number that minimized the mean squared error (MSE) of regression. To

evaluate the predictive performance of the model and minimize overfitting, a 20-fold cross-validation approach was employed. The spectral dataset was randomly partitioned into 20 equal-sized folds, where each fold served as a validation set once while the model was trained on the remaining 19 folds. This process was repeated for all 20 iterations, ensuring that every data point was predicted using a model that had not seen it during training. The resulting cross-validated predictions provide an unbiased estimate of the model's generalization ability.

RESULTS AND DISCUSSION

Monitoring enzyme-catalyzed L-DOPA oxidation kinetics using SERS. HRP, a heme peroxidase commonly found in plants, fungi, and bacteria,[15] can be activated by H_2O_2, forming complex with oxidation potential of 950 mV, [16] and thereby catalyzing oxidation of various reducing substrates, such as phenols, hydroquinones, anilines, etc.[17, 18] L-DOPA, a precursor for dopamine, is a catecholamine commonly used as an oxidation substrate.[19, 20] In the absence of HRP, SERS signals of L-DOPA were immediately observed after mixing L-DOPA, H_2O_2, and AuNPs at 0 min (Fig. 2a) due to the strong affinity of L-DOPA for AuNP surfaces. At pH between 2.32 and 8.67, the L-DOPA molecule existed as a zwitterion, bearing both a positive charge on its amino group and a negative charge on its carboxylic group.[21, 22] The isoelectric point of L-DOPA is 5.51, at which the concentrations of cationic and anionic form are identical. Therefore, L-DOPA at pH 5 is slightly positively charged, which binds effectively to the negatively charged surfaces of AuNPs at high concentration (25 mM). This electrostatic attraction of L-DOPA onto AuNP surfaces results in slight AuNP aggregation, producing observable SERS signals.

The signature "trident-shape" Raman bands of L-DOPA between 1200 and 1600 cm^{-1} were assigned as the C-O stretching of phenolate (1290 cm^{-1}) and the C-C stretching vibrations of

benzene ring (ν_{19a} for 1428 cm^{-1} and ν_{8a} for 1580 cm^{-1}).[23-31] Our negative control experiments show that these "trident-shape" Raman bands are indeed from L-DOPA (Fig. S1&S2). The shape of the "trident", i.e., the relative intensity of these three bands, reflects the oxidation status of L-DOPA. At 0 min, the 1290 cm^{-1} band showed significantly higher intensity, while the other two bands had similar intensities (Fig. 2a). In the absence of HRP, the 1290 cm^{-1} band's intensity slightly decreased in 1 hr relative to the other two bands, suggesting limited oxidation of the phenolic group by H_2O_2 (Fig. 2a).[32-34]

At a low HRP concentration (1 mg/L), oxidation was slow with only slight decreases in the intensities of 1290 and 1428 cm^{-1} bands (Fig. S3). Increasing HRP concentraion to 5 mg/L accelerated oxidation, causing the 1290 cm^{-1} band to drop rapidly within 1 hr, eventually falling below the other two, while the 1580 cm^{-1} band also started to decrease and broaden (Fig. 2b). At 15 mg/L, the oxidaiton rates of 1428 and 1580 cm^{-1} bands became nearly identical, resulting in simultaneous intensity decreases (Fig. 2c). With HRP concentration further increased to 30 and 60 mg/L, the oxidation rate of the 1580 cm^{-1} band surpassed that of the 1428 cm^{-1} band (Fig. 2d-e). At 60 mg/L, the intensity ratio between the bands at 1428 and 1580 cm^{-1} peaked at 30 min and then declined over the remaining 30 min, indicating further oxidation of the benzene ring. At the highest concentration tested (100 mg/L), the 1580 cm^{-1} band intensity rapidly decreased relative to the 1428 cm^{-1} band within the first 15 min, followed by a decrease in the intensity ratio between 1428 and 1580 cm^{-1} bands over the next 45 min (Fig. 2f). Similar trends were repeatedly observed in triplicate measurements (Fig. S4&S5).

Comparable to HRP, Fe^{2+} can catalyze the generation of hydroxyl radicals from H_2O_2 for organic oxidation via the Fenton reaction.[16, 35] Immediately upon Fe^{2+} addition (i.e., 0 min), the 1290 and 1580 cm^{-1} bands have already started to decrease (Fig. S6 and Fig. 2a), indicating the stronger

oxidation capacity of Fenton reaction than HRP-mediated oxidation. Over 1 hr, the intensity of the phenolic group band at 1290 cm^{-1} decreased dramatically, while the intensity ratio between bands at 1428 and 1580 cm^{-1} decreased, which is consistent with the L-DOPA oxidation kinetics observed at a high HRP concentration (i.e., 100 mg/L) (Fig. S6 and Fig. 2f).

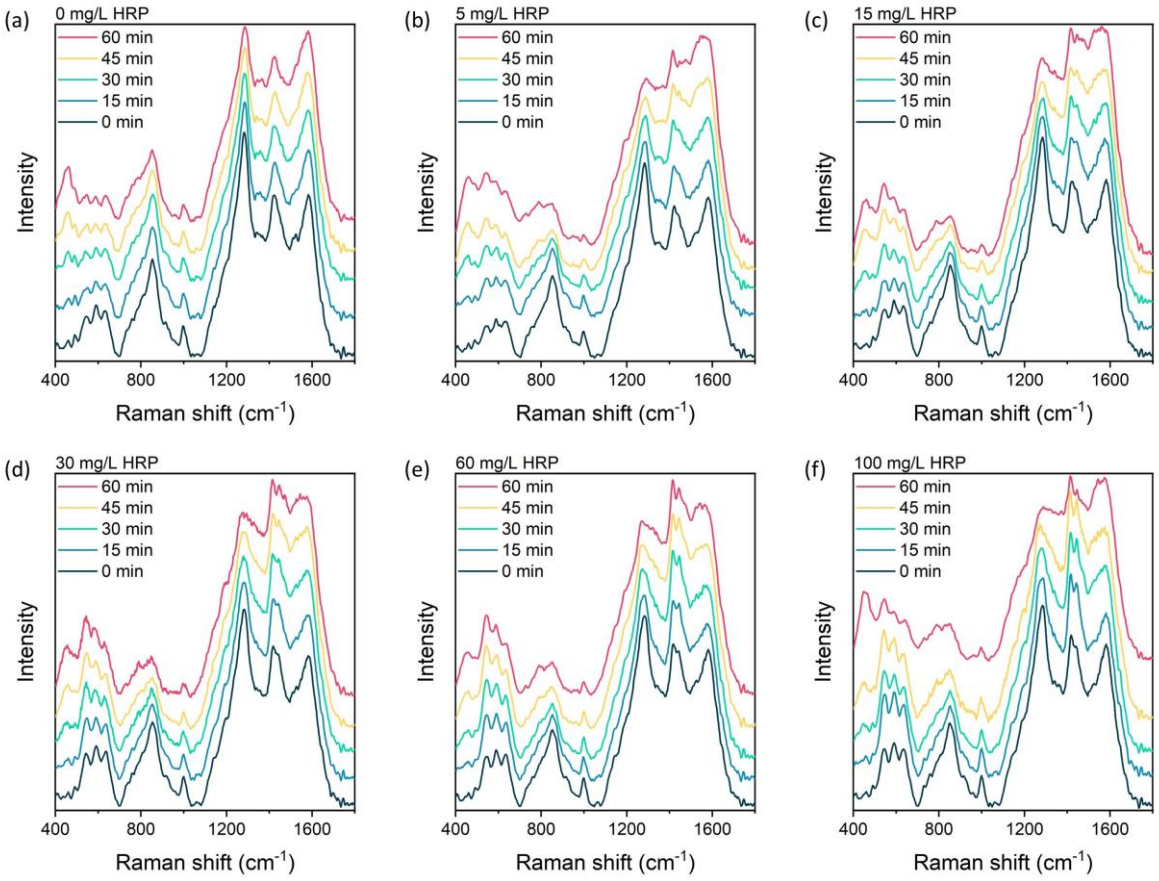

Figure 2. Variation of SERS spectra of L-DOPA over 1 hr, acquired from AuNP colloid containing acetate buffer, L-DOPA, H_2O_2, with varying concentrations of HRP: (a) 0, (b) 5, (c) 15, (d) 30, (e) 60, and (f) 100 mg/L.

PPO specifically catalyzes the oxidation of o-diphenol in L-DOPA to quinone in the presence of oxygen.[36] At low or absent PPO concentrations (0-5 mg/L), the Raman spectra of L-DOPA showed

minimal changes after 1 hr (Fig. S7a-c), indicating the limited oxidation capacity under these circumstances. As PPO concentration increased to 15 mg/L and above, the relative intensity of the 1290 cm^{-1} band steadily decreased compared to the bands at 1428 and 1580 cm^{-1} (Fig. S7d-g), with the 1290 cm^{-1} band nearly disappearing after 1 hr at 60 mg/L PPO (Fig. S7f). The decrease reflects the rapid oxidation of phenolic groups catalyzed by higher PPO concentrations. Similar to HRP, the 1580 cm^{-1} band broadened after 1 hr (Fig. S7e-g), likely due to quinone formation.[37-39] Consistent results from triplicate PPO experiments are shown in Fig. S8-9. Collectively, these PPO and HRP experiments demonstrate the capability of SERS to monitor the oxidation kinetics of model substrate mediated by the extracellular enzymes *in situ* and in real time.

Quantifying soil enzyme activity using L-DOPA Raman spectra. In this section, we aim to quantify the activity of two typical soil enzymes (i.e., HRP and PPO) based on the SERS spectra of L-DOPA during enzyme-catalyzed oxidation processes. Due to the complexity of variations in L-DOPA SERS spectra during oxidation as aforementioned, it was insufficient to simply rely on one single Raman band intensity for quantitative analysis. Instead, a multivariate statistic model based on partial least squares regression was developed to relate the Raman spectrum of L-DOPA to enzyme concentration. Initially, when the input dataset only consisted of spectral data acquired after 60-min oxidation across varying enzyme concentrations (n = 21), the optimal principal number of component was determined to be 6 for HRP (Fig. S10a) and 2 for PPO (Fig. S10c) to achieve the minimum MSEs. While the PLS regression results were acceptable, cross-validation scores were not satisfactory due to the limited sample size (Fig. S10b&d). To overcome this drawback, the 45-min data were incorporated to expand the dataset (n = 42). For HRP, the smallest MSE occurred when component number was 19 (Fig. S11) but minimal change in MSE was observed beyond 8 components. To prevent overfitting, component number of 8 was selected for

PLS modeling. Predicted HRP concentrations were fitted with a polynomial trendline (blue line, Fig. 3) for comparison with the 1:1 reference line (gray dashed line, Fig. 3). The PLS model demonstrated improved fitting and cross-validation performance for HRP (Fig. 3, $R^2 = 0.983$, $R^2_{cv} = 0.837$), confirming the relaibility of this model. Similarly, model performance remained satisfactory for PPO (Fig. S12a&b, $R^2 = 0.865$, $R^2_{cv} = 0.836$).

To further enhance the consistency of this model, additional spectral data collected at 30, 15, and 0 min were incrementally included (n = 63, 84, and 105), with PLS regression applied correspondingly. Error analysis and PLS modeling results are shown in Fig. S13-15. Incorporating the “30 min” and “15 min” datasets led to minimal change in PLS model fitting performance for HRP (Fig. S13a&b, Fig. S14a&b). However, adding the “0 min” data significantly reduced both model fitting and validation performance (Fig. S15a&b). For PPO, model fitting improved with the data earlier than 45 min included, while the number of optimal principal component increased from 2 to 9-10 (Fig. S13-15 c&d).

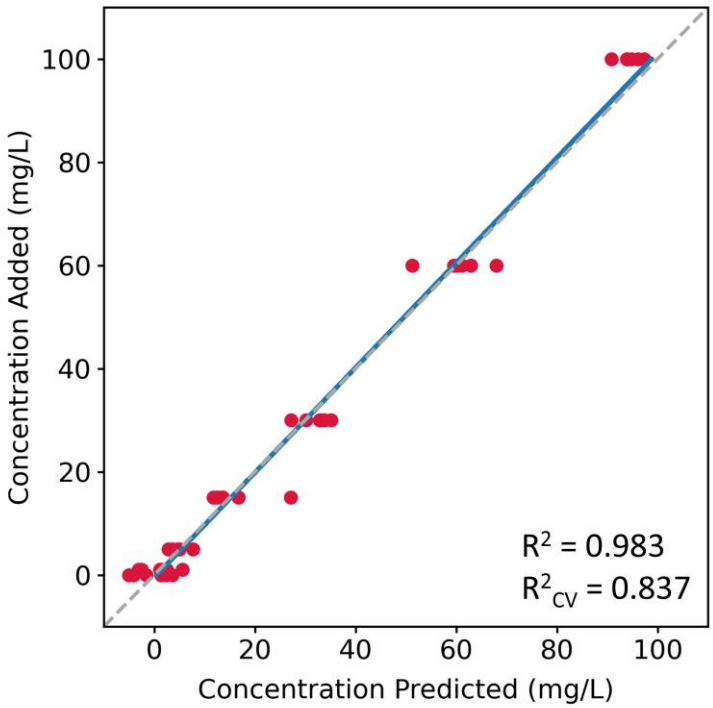

Figure 3. Relationship between the concentration of added HRP and the predicted HRP concentration using a PLS regression model. The PLS regression model was trained to correlate the SERS spectra of L-DOPA after oxidation with HRP concentration combining data collected at 45 and 60 min. "CV" refers to cross validation.

CONCLUSIONS

To apply the SERS sensor and PLS regression model to real soil samples, we collected 117 samples across diverse soil types in Nashville, TN (Fig. 4a), including farmlands, grasslands, woodlands, wetland, and gardens. Following collection, both conventional colorimetric enzyme activity measurement and SERS sensing were promptly performed. The conventional assay quantified enzyme activity based on the mass of L-DOPA oxidized at optimum temperature. The PLS regression model was established by correlating the normalized SERS spectrum of L-DOPA after 60-min of oxidation with enzyme activity measured via the standard colorimetric assay. The

optimal principal component number was determined to be 8 when the minimal MSE was achieved (Fig. S16). Although the model's performance was lower than those observed for pure enzyme samples in the laboratory, it still demonstrated satisfactory fitting for real soil samples (Fig. 4b, R^2 = 0.753) and reasonable generalizability upon cross-validation (Fig. 4b, R^2_{cv} = 0.351), despite the inherent heterogeneity of the samples. The compromised performance is likely attributable to the complex nature of soil matrices and extracellular enzymes, which are affected by diverse vegetation types and exhibit significant spatial and temporal variability. Contributing factors include heterogeneity in soil composition (e.g., organic matter content, pH, and ionic strength), arising from differences in sampling location and depth, which can influence analyte adsorption and nanoparticle aggregation. Moreover, humic substances and other matrix components may interfere with Raman signal acquisition, while biological variability, including differences in microbial communities and enzyme isoforms, can further impact enzyme activity measurements.

Despite these challenges, this preliminary field study demonstrates the strong potential of SERS for *in-situ*, real-time sensing of soil enzyme activities using portable instrumentation, an advantage not achievable with conventional colorimetric assays. The method enables analysis within 1.5 hours without requiring temperature-controlled incubation or specialized laboratory equipment, and this timeframe could potentially be reduced to minutes as future datasets help account for uncertainties associated with reaction kinetics. Selectivity toward specific enzymes can be introduced through the addition of H_2O_2, which is required for peroxidase catalysis but not for oxidases, allowing for differential response profiling and better resolution between enzyme classes. In terms of sensitivity, the method reliably detected enzyme concentration as low as 1 mg/L, and model predictions aligned well with activity levels observed in real soil samples, demonstrating its relevance for environmental applications. These findings underscore the potential for selective

and sensitive detection of extracellular enzyme activity in complex soil matrices. Future improvements, including site- and depth-specific calibration, expanded training datasets, and integration of auxiliary soil parameters, will further enhance model robustness and field accuracy. Overall, this work lays the foundation for scalable, cost-effective monitoring of soil enzyme activities to support environmental research and sustainable land management.

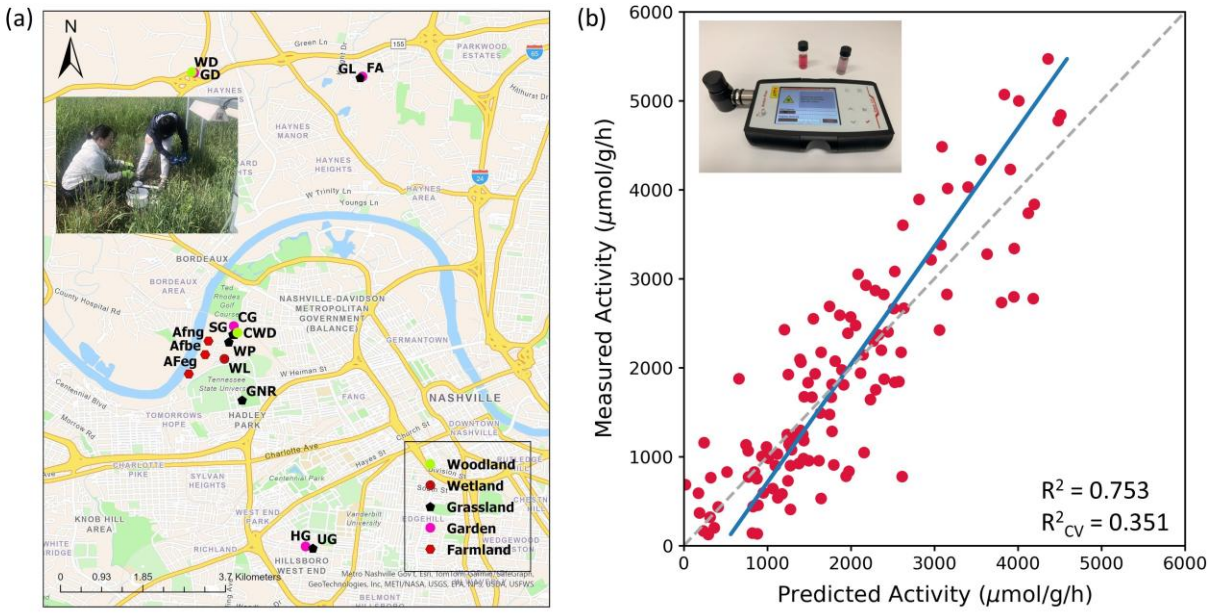

Figure 4. (a) Map of sampling site locations, with an inset showing a photo of our team during field sampling in Nashville, TN; (b) Correlation between soil enzyme activity measured by the traditional colorimetric method and predicted values from the PLS regression model based on SERS measurement. “CV” refers to cross validation. The inset shows a photo of the portable Raman spectrometer used in this study.

CONFLICTS OF INTEREST

The authors declare no competing financial interest.

DATA AVAILABILITY

This study does not include any data supporting the results from published papers and external databases. The in-house Python code for PLS analysis can be accessed using the following Github link: https://github.com/hwang166/PLS-Code

ACKNOWLEDGEMENTS

The authors would like to thank the support from the United States Department of Agricultural National Institute of Food & Agriculture (2023-67021-39748). Additional support for Hanwei Wang was provided by the Wisconsin Alumni Research Foundation (WARF). Funds to Li is from a USDA National Institute of Food and Agriculture (NIFA) Foundational and Applied Science Program (No. 2021-67020-34933), a National Science Foundation Collaborative Research GP-GO (#2232215), a Department of Energy RRDP grant (#DE-SC0023206), and a USDA Evans-Allen grant (#222725). The authors would like to thank Xuehan Wang and Dr. Jiacong Zhou for their help in soil sample collection and treatment.

REFERENCES

1. D. A. Bossio, S. C. Cook-Patton, P. W. Ellis, J. Fargione, J. Sanderman, P. Smith, S. Wood, R. J. Zomer, M. von Unger, I. M. Emmer and B. W. Griscom, The Role of Soil Carbon in Natural Climate Solutions, *Nat. Sustain.*, 2020, **3**, 391-398.
2. M. A. Bradford, C. J. Carey, L. Atwood, D. Bossio, E. P. Fenichel, S. Gennet, J. Fargione, J. R. B. Fisher, E. Fuller, D. A. Kane, J. Lehmann, E. E. Oldfield, E. M. Ordway, J. Rudek, J. Sanderman and S. A. Wood, Soil Carbon Science for Policy and Practice, *Nat. Sustain.*, 2019, **2**, 1070-1072.
3. R. G. Burns, J. L. DeForest, J. Marxsen, R. L. Sinsabaugh, M. E. Stromberger, M. D. Wallenstein, M. N. Weintraub and A. Zoppini, Soil Enzymes in a Changing Environment: Current Knowledge and Future Directions, *Soil Biol. Biochem.*, 2013, **58**, 216-234.
4. R. L. Sinsabaugh, Phenol Oxidase, Peroxidase and Organic Matter Dynamics of Soil, *Soil Biol. Biochem.*, 2010, **42**, 391-404.
5. R. L. Sinsabaugh, R. K. Antibus and A. E. Linkins, An Enzymic Approach to the Analysis of Microbial Activity during Plant Litter Decomposition, *Agric. Ecosyst. Environ.*, 1991, **34**, 43-54.
6. R. L. Sinsabaugh and D. L. Moorhead, Resource Allocation to Extracellular Enzyme Production: A Model for Nitrogen and Phosphorus Control of Litter Decomposition, *Soil Biol. Biochem.*, 1994, **26**, 1305-1311.
7. A. C. Brangarí, S. Manzoni and J. Rousk, A Soil Microbial Model to Analyze Decoupled Microbial Growth and Respiration during Soil Drying and Rewetting, *Soil Biol. Biochem.*, 2020, **148**, 107871.

8. K. Kneipp, H. Kneipp, I. Itzkan, R. R. Dasari and M. S. Feld, Ultrasensitive Chemical Analysis by Raman Spectroscopy, *Chem. Rev.*, 1999, **99**, 2957-2976.

9. R. M. Stockle, Y. D. Suh, V. Deckert and R. Zenobi, Nanoscale Chemical Analysis by Tip-Enhanced Raman Spectroscopy, *Chem. Phys. Lett.*, 2000, **318**, 131-136.

10. R. A. Halvorson and P. J. Vikesland, Surface-Enhanced Raman Spectroscopy (SERS) for Environmental Analyses, *Environ. Sci. Technol.*, 2010, **44**, 7749-7755.

11. H. Wei, W. Leng, J. Song, M. R. Willner, L. C. Marr, W. Zhou and P. J. Vikesland, Improved Quantitative SERS Enabled by Surface Plasmon Enhanced Elastic Light Scattering, *Anal. Chem.*, 2018, **90**, 3227-3237.

12. H. Wang, A. Kvit and H. Wei, In Situ Monitoring of the Polymerization Kinetics of Organic Pollutants during Persulfate-Based Advanced Oxidation Processes Using Plasmonic Colorimetry, *Anal. Chem.*, 2024, **96**, 1587-1596.

13. R. L. Sinsabaugh, K. Saiya-Cork, T. Long, M. P. Osgood, D. A. Neher, D. R. Zak and R. J. Norby, Soil Microbial Activity in a Liquidambar Plantation Unresponsive to CO_2-Driven Increases in Primary Production, *Appl. Soil Ecol.*, 2003, **24**, 263-271.

14. K. R. Saiya-Cork, R. L. Sinsabaugh and D. R. Zak, The Effects of Long Term Nitrogen Deposition on Extracellular Enzyme Activity in an Acer Saccharum Forest Soil, *Soil Biol. Biochem.*, 2002, **34**, 1309-1315.

15. J. N. Rodríguez-López, D. J. Lowe, J. Hernández-Ruiz, A. N. P. Hiner, F. García-Cánovas and R. N. F. Thorneley, Mechanism of Reaction of Hydrogen Peroxide with Horseradish Peroxidase: Identification of Intermediates in the Catalytic Cycle, *J. Am. Chem. Soc.*, 2001, **123**, 11838-11847.

16. B. L. Allen, G. P. Kotchey, Y. Chen, N. V. K. Yanamala, J. Klein-Seetharaman, V. E. Kagan and A. Star, Mechanistic Investigations of Horseradish Peroxidase-Catalyzed Degradation of Single-Walled Carbon Nanotubes, *J. Am. Chem. Soc.*, 2009, **131**, 17194-17205.

17. B. Kalra and R. A. Gross, Horseradish Peroxidase Mediated Free Radical Polymerization of Methyl Methacrylate, *Biomacromolecules*, 2000, **1**, 501-505.

18. Q. Huang, Q. Huang, R. A. Pinto, K. Griebenow, R. Schweitzer-Stenner and W. J. Weber, Inactivation of Horseradish Peroxidase by Phenoxyl Radical Attack, *J. Am. Chem. Soc.*, 2005, **127**, 1431-1437.

19. K. Jodko-Piórecka, B. Sikora, M. Kluzek, P. Przybylski and G. Litwinienko, Antiradical Activity of Dopamine, L-DOPA, Adrenaline, and Noradrenaline in Water/Methanol and in Liposomal Systems, *J. Org. Chem.*, 2022, **87**, 1791-1804.

20. J. Haavik, L-DOPA Is a Substrate for Tyrosine Hydroxylase, *J. Neurochem.*, 1997, **69**, 1720-1728.

21. S. Miyamoto and C. L. A. Schmidt, The Apparent Dissociation Constants of Phenylalanine and of Dihydroxyphenylalanine and the Apparent Free Energy and Entropy Changes of Certain Amino Acids Due to Ionization, *J. Biol. Chem.*, 1931, **90**, 165-178.

22. X. Chen, J. Zhang, H. Zhai, X. Chen and Z. Hu, Determination of Levodopa by Capillary Zone Electrophoresis Using an Acidic Phosphate Buffer and Its Application in the Analysis of Beans, *Food Chem.*, 2005, **92**, 381-386.

23. S. J. Hurst, H. C. Fry, D. J. Gosztola and T. Rajh, Utilizing Chemical Raman Enhancement: A Route for Metal Oxide Support-Based Biodetection, *J. Phys. Chem. C*, 2011, **115**, 620-630.

24. J. Feng, H. Fan, D.-a. Zha, L. Wang and Z. Jin, Characterizations of the Formation of Polydopamine-Coated Halloysite Nanotubes in Various pH Environments, *Langmuir*, 2016, **32**, 10377-10386.

25. M. L. Mcglashen, K. L. Davis and M. D. Morris, Surface-Enhanced Raman-Scattering of Dopamine at Polymer-Coated Silver Electrodes, *Anal. Chem.*, 1990, **62**, 846-849.

26. M. Jaber, M. Bouchoucha, L. Delmotte, C. Méthivier and J.-F. Lambert, Fate of L-DOPA in the Presence of Inorganic Matrices: Vectorization or Composite Material Formation?, *J. Phys. Chem. C*, 2011, **115**, 19216-19225.

27. M. Kaya and M. Volkan, New Approach for the Surface Enhanced Resonance Raman Scattering (SERRS) Detection of Dopamine at Picomolar (pM) Levels in the Presence of Ascorbic Acid, *Anal. Chem.*, 2012, **84**, 7729-7735.

28. N. S. Lee, Y. Z. Hsieh, R. F. Paisley and M. D. Morris, Surface-Enhanced Raman Spectroscopy of the Catecholamine Neurotransmitters and Related Compounds, *Anal. Chem.*, 1988, **60**, 442-446.

29. B. Edwin and I. Hubert Joe, Vibrational Spectral Analysis of Anti-Neurodegenerative Drug Levodopa: A Dft Study, *J. Mol. Struct.*, 2013, **1034**, 119-127.

30. M. Spasovová, J. Kapitán, S. Jílek, M. S. P. Kkadan, J. Klener, N. J. r. Lynn, V. J. r. Kopecky, V. Baumruk and V. Profant, Probing Solution Conformations of L-DOPA: Integration of Experiment and Simulation Via Vibrational Optical Activity, *Spectrochim. Acta A Mol. Biomol. Spectrosc.*, 2024, **313**.

31. S. Pande, S. Jana, A. K. Sinha, S. Sarkar, M. Basu, M. Pradhan, A. Pal, J. Chowdhury and T. Pal, Dopamine Molecules on Aucore−Agshell Bimetallic Nanocolloids: Fourier

Transform Infrared, Raman, and Surface-Enhanced Raman Spectroscopy Study Aided by Density Functional Theory, *J. Phys. Chem. C*, 2009, **113**, 6989-7002.

32. Y. Cheneviere, V. Caps and A. Tuel, Gold-Catalyzed Oxidation of Substituted Phenols by Hydrogen Peroxide, *Appl. Catal. A: Gen.*, 2010, **387**, 129-134.

33. H. Wei, S. K. Loeb, N. J. Halas and J.-H. Kim, Plasmon-Enabled Degradation of Organic Micropollutants in Water by Visible-Light Illumination of Janus Gold Nanorods, *Proc. Natl. Acad. Sci. U.S.A.*, 2020, **117**, 15473-15481.

34. T. Ishida, K. Kuroda, N. Kinoshita, W. Minagawa and M. Haruta, Direct Deposition of Gold Nanoparticles onto Polymer Beads and Glucose Oxidation with H_2O_2, *J. Colloid Interface Sci.*, 2008, **323**, 105-111.

35. C. Merino, Y. Kuzyakov, K. Godoy, P. Cornejo and F. Matus, Synergy Effect of Peroxidase Enzymes and Fenton Reactions Greatly Increase the Anaerobic Oxidation of Soil Organic Matter, *Sci. Rep.*, 2020, **10**, 11289.

36. S. Araji, T. A. Grammer, R. Gertzen, S. D. Anderson, M. Mikulic-Petkovsek, R. Veberic, M. L. Phu, A. Solar, C. A. Leslie, A. M. Dandekar and M. A. Escobar, Novel Roles for the Polyphenol Oxidase Enzyme in Secondary Metabolism and the Regulation of Cell Death in Walnut, *Plant Physiol.*, 2014, **164**, 1191-1203.

37. M. Zhu, X. Huang, J. Li and H. Shen, Peroxidase-Based Spectrophotometric Methods for the Determination of Ascorbic Acid, Norepinephrine, Epinephrine, Dopamine and Levodopa, *Anal. Chim. Acta*, 1997, **357**, 261-267.

38. R. P. Ferrari, E. Laurenti, L. Casella and S. Poli, Oxidation of Catechols and Catecholamines by Horseradish Peroxidase and Lactoperoxidase: ESR Spin Stabilization

Approach Combined with Optical Methods, *Spectrochim. Acta A Mol. Biomol. Spectrosc.*, 1993, **49**, 1261-1267.

39. M. Puiu, I. Babaligea, C. Olmazu, A. Răducan and D. Oancea, Peroxidase-Mediated Oxidation of L-Dopa: A Kinetic Approach, *Biochem. Eng. J.*, 2010, **52**, 248-254.

DATA AVAIALBILITY STATEMENT

This study does not include any data supporting the results from published papers and external databases. The in-house Python code for PLS analysis can be accessed using the following Github link: https://github.com/hwang166/PLS-Code